FERMILAB-PUB-20-513-T

The low-energy constant L_{10} in a two-representation lattice theory

Maarten Golterman,[1] William I. Jay,[2] Ethan T. Neil,[3] Yigal Shamir,[4,*] and Benjamin Svetitsky[4]

[1] *Department of Physics and Astronomy, San Francisco State University, San Francisco, CA 94132, USA*

[2] *Theoretical Physics Department, Fermi National Accelerator Laboratory, Batavia, Illinois, 60510, USA*

[3] *Department of Physics, University of Colorado, Boulder, CO 80309, USA*

[4] *Raymond and Beverly Sackler School of Physics and Astronomy, Tel Aviv University, 69978 Tel Aviv, Israel*

(Dated: April 2, 2021)

Abstract

We calculate the low-energy constant L_{10} in a two-representation SU(4) lattice gauge theory that is close to a composite-Higgs model. From this we obtain the contribution of the new strong sector to the S parameter. This leads to an upper bound on the vacuum misalignment parameter ξ which is similar to current estimates of this bound. Our result agrees with large-N_c scaling expectations, within large systematic uncertainties.

* shamir@tauex.tau.ac.il

I. INTRODUCTION

The composite-Higgs paradigm [1, 2] provides a solution to the problem of protecting the Higgs mass from large radiative corrections by supposing that the Higgs is a pseudo Nambu-Goldstone boson (pNGB) of some new strong interaction, dubbed hypercolor, operative at the few-TeV scale. Often, one also supposes that the top quark is partially composite, meaning that it acquires its large mass by mixing with a top partner—a baryon of the new strong force with the same Standard Model quantum numbers [3] (for reviews, see Refs. [4–6]).

A number of concrete realizations of the composite-Higgs scenario, based on asymptotically free gauge theories, were proposed some time ago in Ref. [7] (see also Refs. [8–10]). In a series of papers [11–15], we have studied the SU(4) gauge theory with two Dirac fermions in the fundamental representation, together with two Dirac fermions—equivalently, 4 Majorana fermions—in the sextet representation, which is a real representation. By itself, this fermion content is not enough to accommodate a composite Higgs along with a top partner. Starting from here, however, we can reach two of the models proposed in Ref. [7]—denoted M6 and M11 in Ref. [10]—by increasing the number of fermion species in each representation. In fact, the fermion content of our model is quite close to that of the M6 model, which has 3 fundamental Dirac fermions together with 5 Majorana sextet fermions. Values of low-energy constants (LECs) calculated in our model may thus be quite close to their values in the M6 model.[1] Our choice of two Dirac fermions in each representation allows us to use the standard hybrid Monte Carlo (HMC) algorithm in our simulations, whereas simulating the actual M6 model would require the more costly rational HMC (RHMC) algorithm (see, for example, Ref. [17]).[2]

In this paper we focus on L_{10}, a next-to-leading order (NLO) LEC which, in chiral perturbation theory (ChPT) for fermions in a single representation, multiplies the operator [19, 20]

$$\mathcal{O}_{10} = -\operatorname{tr}\left((\mathcal{V}_{\mu\nu} - \mathcal{A}_{\mu\nu})\Sigma(\mathcal{V}_{\mu\nu} + \mathcal{A}_{\mu\nu})\Sigma^\dagger\right) \ . \tag{1.1}$$

In the current model, as well as in the M6 model, Σ is the non-linear field for pNGBs made out of the sextet fermions; by analogy with QCD, we will often refer to these pNBGs as "pions."[3] $\mathcal{V}_{\mu\nu}$ and $\mathcal{A}_{\mu\nu}$ are the field strengths of external gauge fields $\mathcal{V}_\mu$ and $\mathcal{A}_\mu$ which, in turn, couple to vector currents V_μ and axial currents A_μ. As in QCD, also for a real representation the vector and axial currents are associated with unbroken and broken flavor generators, respectively. For more details, we refer to App. A. As we discuss in detail below, L_{10} can be extracted from $\langle V_\mu V_\nu - A_\mu A_\nu\rangle$, the difference between the connected two-point functions of the vector and axial currents.[4]

This paper is organized as follows. In Sec. II we give the necessary theoretical background. In Sec. III we describe the extraction of L_{10} from our mixed-action lattice calculations. Using only our smallest valence mass, we first present NLO fits that give good results for L_{10}. We then estimate the systematic error in L_{10} by considering fits that include a selection of NNLO analytic terms to data from all our valence masses. In Sec. IV we use L_{10} and the experimental value of the S parameter [22, 23] to obtain a bound on the scale

[1] In QCD, values of LECs typically change by a small amount when increasing the number of light flavors in the simulation from 2 to 3 [16].

[2] The M11 model has 4 fundamental Dirac fermions and 6 Majorana sextet fermions. We note that the Sp(4) gauge theory, on which models M5 and M8 are based, is also currently under study [18].

[3] ChPT for two fermion representations was developed in Ref. [21].

[4] Another interesting LEC that can be extracted from $\langle V_\mu V_\nu - A_\mu A_\nu\rangle$ is C_{LR}, which we have calculated previously [15].

of the hypercolor theory, and we summarize. In App. A we briefly review the embedding of the electroweak gauge fields of the Standard Model in the M6 composite-Higgs model [8, 9, 24, 25], and calculate the contribution of the hypercolor theory to the S parameter. Some technical details regarding discretization effects in ChPT are relegated to App. B, while some further investigations of our lattice data are described in App. C.

II. THEORETICAL BACKGROUND

In this section we summarize the theoretical background for our calculation. In Sec. II A we give the basic definitions, and discuss partially-quenched ChPT at NLO. In Sec. II B we discuss corrections beyond NLO, and in Sec. II C we discuss lattice discretization effects. For relevant ChPT literature, see Refs. [19–21, 26–31]. For reviews, see Refs. [32, 33].

A. Partially-quenched chiral perturbation theory at next-to-leading order

We begin with the two-point function of the vector-current,

$$\delta_{ab}\Pi_{VV,\mu\nu}(q) = \int d^4x\, e^{iqx}\, \langle V_{\mu a}(x) V_{\nu b}(0)\rangle \ , \tag{2.1}$$

and we define the axial-current correlator $\Pi_{AA,\mu\nu}$ similarly. We express their difference in terms of two invariant functions,

$$\begin{aligned} \Pi_{LR,\mu\nu}(q) &= \Pi_{VV,\mu\nu}(q) - \Pi_{AA,\mu\nu}(q) \\ &= (q^2\delta_{\mu\nu} - q_\mu q_\nu)\Pi^{(1)}(q^2) + q_\mu q_\nu \Pi^{(0)}(q^2) \ . \end{aligned} \tag{2.2}$$

The transverse part, $\Pi^{(1)}(q^2)$, is an order parameter for chiral symmetry breaking. Having in hand our lattice calculation of $\Pi^{(1)}$ [15], we compare in Sec. III the results with the predictions of ChPT. We make similar use of the difference

$$\Pi^{(1-0)} = \Pi^{(1)} - \Pi^{(0)} \ . \tag{2.3}$$

Our lattice calculation is based on different lattice formulations for the sea and valence fermions (see Sec. II C below), and we also allow for different sea and valence masses. We are thus forced to consider partially-quenched (PQ) ChPT. Setting aside lattice corrections for now, we find that continuum PQ ChPT gives pole terms in leading order (LO),

$$\Pi^{(1)} = \frac{F_{vv}^2}{q^2} + \hat{\Pi}^{(1)} \ , \tag{2.4}$$

and

$$\Pi^{(1-0)} = \frac{F_{vv}^2}{q^2 + M_{vv}^2} + \hat{\Pi}^{(1)} \ , \tag{2.5}$$

where $\hat{\Pi}^{(1)}$ first arises in NLO. The poles arise from the creation and annihilation of a single valence pion; M_{vv} and F_{vv} are the valence pion mass and decay constant, respectively. The $1/q^2$ singularity in $\Pi^{(1)}$ is kinematical, and so its location is independent of M_{vv}.

In NLO, $\hat{\Pi}^{(1)}$ arises from a pion loop, which introduces L_{10} as a counterterm. In our case, the loop is made of a mixed sea-valence pion. Explicitly,

$$\hat{\Pi}^{(1)}(q^2) = \frac{\mathcal{G}(N)}{48\pi^2}\left[\frac{1}{3} + \log\left(\frac{M_{vs}^2}{\mu^2}\right) - H(s)\right] + 8L_{10} \ . \tag{2.6}$$

The ingredients of the NLO expression are the following. For $N = 2$ Dirac fermions in a real representation, the group theoretical factor is $\mathcal{G}(N) = N + 1 = 3$ [20]. In the continuum, the mass of the mixed pion is given to LO by

$$M_{vs}^2 = \left(M_{ss}^2 + M_{vv}^2\right)/2 \ , \tag{2.7}$$

where M_{ss} is the mass of the sextet sea pion. Finally, the function $H(s)$ is given by

$$H(s) = 2s^2 + s^3 \log\left(\frac{s-1}{s+1}\right) , \tag{2.8}$$

where in turn

$$s = \sqrt{1 + 4M_{vs}^2/q^2} \ . \tag{2.9}$$

We use the same renormalization prescription for loop diagrams as in Refs. [20, 27]. We choose the renormalization scale to be $\mu^2 = 1/t_0$, where t_0 is the gradient-flow scale [34].

Each of our lattice ensembles gives us values for $\Pi^{(1)}(q^2)$ and $\Pi^{(1-0)}(q^2)$ in a range of momenta q and for a set of values of the valence fermion mass, giving two different approaches to $\hat{\Pi}^{(1)}(q^2)$ via Eqs. (2.4) and (2.5); $\hat{\Pi}^{(1)}(q^2)$ is supposed to satisfy Eq. (2.6), subject to NNLO and lattice corrections, described below. Likewise, each ensemble gives M_{vv} and F_{vv}, again as a function of the valence fermion mass, as well as an ensemble average of M_{ss}. Then a fit to $\Pi^{(1)}(q^2)$ or $\Pi^{(1-0)}(q^2)$ gives L_{10}.

B. Beyond next-to-leading order

The earliest determination of L_{10} in QCD was based on experimental input [19]. The first lattice calculations, using ChPT at NLO, gave a similar value [35, 36]. The much more challenging calculation at next-to-NLO (NNLO) was performed by two groups [37, 38] several years later (see also Ref. [16]). The NNLO calculations, which combined lattice results with experimental data, found a central value lower by some 30% than the early NLO calculations.

In the continuum, an NNLO calculation of $\Pi^{(1)}$ and $\Pi^{(1-0)}$ in the PQ theory will contain new loop diagrams, along with counterterms of the form

$$\frac{1}{(4\pi F)^2}\left(b_q q^2 + b_s m_s + b_v m_v\right) \ . \tag{2.10}$$

Here m_s and m_v are the masses of the sextet sea and valence fermions, and the parameters b_q, b_s and b_v are linear combinations of the NNLO LECs. F is the sextet pion decay constant in the chiral limit. A full NNLO calculation is beyond the scope of this work; nonetheless, in view of the lesson from QCD calculations, we attempt below to estimate the systematic uncertainties of our calculation by exploring the effect of analytic terms similar in structure to the NNLO counterterms.

In principle, Eq. (2.10) should contain an additional term proportional to the mass of the fundamental-representation sea fermions, $m_{s,4}$. We have found in previous work, however, that $m_{s,4}$ has almost no effect on observables constructed from the sextet fermions [11], and hence we drop it.

C. Lattice discretization

Our lattice simulations employed Wilson fermions for the dynamical sea: two flavors in the fundamental representation, along with two (Dirac) flavors in the sextet representation [11]. Because of the importance of chiral symmetry for the calculation of $\Pi_{LR,\mu\nu}(q)$, we constructed the current correlators using staggered valence fermions [15]. These are much more economical than other chiral fermion formulations—overlap and domain-wall—that have been used for calculations of L_{10} in QCD [35, 36].

We calculated the connected part of the vector and axial two-point functions as follows. At a formal level, we introduce two valence staggered fields in the sextet representation, and consider the flavor non-singlet vector currents (see for example Ref. [39]). These are[5]

$$V_{\mu a}(x) = \frac{\eta_\mu(x)}{2}\left[\bar\chi(x)U_\mu(x)T_a\chi(x+\hat\mu) + \bar\chi(x+\hat\mu)U_\mu^\dagger(x)T_a\chi(x)\right] \ , \tag{2.11}$$

defined from one-component staggered fields $\chi, \bar\chi$. Here $U_\mu(x)$ is the SU(4) lattice gauge field. The corresponding partially conserved axial currents include the sign factor $\epsilon(x) = (-1)^{x_1+x_2+x_3+x_4}$, and are given by

$$A_{\mu a}(x) = \frac{\eta_\mu(x)\epsilon(x)}{2}\left[\bar\chi(x)U_\mu(x)T_a\chi(x+\hat\mu) - \bar\chi(x+\hat\mu)U_\mu^\dagger(x)T_a\chi(x)\right] \ . \tag{2.12}$$

The other sign factors are, as usual,

$$\eta_1(x) = 1 \ , \quad \eta_2(x) = (-1)^{x_1} \ , \quad \eta_3(x) = (-1)^{x_1+x_2} \ , \quad \eta_4(x) = (-1)^{x_1+x_2+x_3} \ . \tag{2.13}$$

These currents correspond to the nearest-neighbor staggered action.

We calculated the current–current correlation function with these staggered currents, and we extracted lattice approximations to the invariant functions by the same method as in Refs. [15, 35, 40]. Introducing the chiral currents, $J^L_{\mu a} = V_{\mu a} - A_{\mu a}$ and $J^R_{\mu a} = V_{\mu a} + A_{\mu a}$, we define the lattice correlator,[6]

$$\delta_{ab}\Pi^{\rm lat}_{\mu\nu}(q) = \frac{1}{4}a^4\sum_x e^{iqx}\ \left\langle J^L_{\mu a}(x)J^R_{\nu b}(0)\right\rangle \ , \tag{2.14}$$

where a is the lattice spacing. The factor of $\frac{1}{4}$ corrects for the summation over the four tastes contained in the staggered field. With $\Pi^{\rm lat}_{\mu\nu}(q)$ in hand, we extract the transverse and longitudinal functions via

$$\Pi^{(1)} = \frac{\sum_{\mu\nu} P^\perp_{\mu\nu}\,\Pi^{\rm lat}_{\mu\nu}}{3(\hat q^2)^2} \ , \tag{2.15}$$

$$\Pi^{(0)} = \frac{\sum_{\mu\nu} P^\parallel_{\mu\nu}\,\Pi^{\rm lat}_{\mu\nu}}{(\hat q^2)^2} \ ,$$

where the lattice projectors are

$$P^\perp_{\mu\nu} = \hat q^2\delta_{\mu\nu} - \hat q_\mu\hat q_\nu \ , \tag{2.16}$$
$$P^\parallel_{\mu\nu} = \hat q_\mu\hat q_\nu \ .$$

[5] Throughout this paper the traceless, hermitian flavor generators are normalized according to $\mathrm{tr}(T_aT_b) = \delta_{ab}$.

[6] Our sign convention here is opposite to that in our earlier paper [15].

Here $\hat{q}_\mu = (2/a)\sin(aq_\mu/2)$, and $\hat{q}^2 = \sum_\mu \hat{q}_\mu^2$. Following common practice, it is also convenient to replace q^2 everywhere by $\hat{q}^2$ in the ChPT results of Sec. II A.

Since we use different sea and valence lattice fermions, we need to generalize the partially-quenched results to mixed-action lattice ChPT. This entails the introduction of two new parameters. First, in place of Eq. (2.7), the mass of the mixed sea-valence pion becomes

$$t_0 M_{vs}^2 = t_0 \left(M_{ss}^2 + M_{vv}^2\right)/2 + \hat{a}^2 \Delta_{\text{mix}} \ , \tag{2.17}$$

where we have expressed all quantities in t_0 units, and $\hat{a} = a/\sqrt{t_0}$. Here Δ_{mix} is a new LO LEC of the mixed-action theory [28–30]. Following the reasoning of Ref. [31], Δ_{mix} must be positive.

In addition, at NNLO there is one more analytic term. The full set of analytic NNLO terms we use is

$$t_0 \left(b_q q^2 + b_{ss} M_{ss}^2 + b_{vv} M_{vv}^2\right) + b_a \hat{a}^2 \ . \tag{2.18}$$

This involves two technical changes compared to Eq. (2.10). First, instead of using the decay constant F for the reference scale, it is more convenient for us to use the gradient flow scale t_0. Also, we replace the term linear in m_s (m_v) by a term linear in M_{ss}^2 (M_{vv}^2), noting that they are interchangeable at LO in ChPT. The new element in Eq. (2.18) is the last term: a discretization term proportional to a^2. In App. B we explain why the discretization term is $\sim a^2$, and not $\sim a$.

III. FITS TO NUMERICAL RESULTS

We begin with a brief description of the ensembles. In this work we use 12 ensembles with volume $16^3 \times 32$, the same set of ensembles we used for our study of the baryon spectrum [12]. In addition, we use 3 ensembles with volume $24^3 \times 48$, numbered 40, 42 and 43 in Ref. [11].[7]

For each ensemble, we calculated the connected two-point function of the (partially) conserved vector and axial staggered currents of the sextet representation for 7 valence masses: $am_v = 0.01$, 0.015, 0.02, 0.025, 0.03, 0.035, and 0.05. We also calculated the mass of the valence staggered (Goldstone) pion, aM_{vv}, and its decay constant aF_{vv}, again as a function of am_v.[8] The sextet (Wilson) sea pion mass, aM_{ss}, and the gradient flow scale t_0/a^2, which are also used in our analysis, were previously obtained in Ref. [11]. Fixing t_0 as the scale of the theory gives us the lattice spacing a for each ensemble: For the present ensemble set, t_0/a^2 is in the range 0.9–2.7, while $\sqrt{t_0}M_{ss}$ is in the range 0.2–0.58. On each ensemble, correlations of all valence observables as well as M_{ss} were calculated using single-elimination jackknife. The only exceptions are correlations of t_0 with other observables, which we ignore because the fluctuations in t_0 are very small.

While all 7 valence masses are ultimately used in our analysis, we restrict our fits to $\Pi^{(1)}(q^2)$ and $\Pi^{(1-0)}(q^2)$ to the smallest momentum (which is timelike on our asymmetric lattices). On the $16^3 \times 32$ lattices, this momentum is $aq \simeq a\hat{q} \simeq 0.196$, roughly equal to our largest valence pion mass at the smallest valence fermion mass ($am_v = 0.01$). The next lattice momentum is $\simeq 0.39$, which is comparable to our valence pion masses for the largest valence fermion mass. As we will see, we cannot include data from the higher valence

[7] A fourth ensemble with this volume turned out to be an outlier, and is not included in our analysis.

[8] All the calculations described to this point—staggered valence spectra and current correlators—were carried out for the analysis of C_{LR} presented in Ref. [15], which can be consulted for further details.

method	p-value	$-L_{10}$	$-\Delta_{\rm mix}$
$\Pi^{(1)}$	0.34	0.0094(6)	0.05(3)
$\Pi^{(1-0)}$	0.32	0.0091(6)	0.06(2)
$\Pi^{(1)}$	0.35	0.0098(5)	–
$\Pi^{(1-0)}$	0.26	0.0096(5)	–

TABLE 1. NLO fits, using data from the smallest valence mass.

fermion masses without an NNLO ingredient in the fit. Aiming to limit other sources of large NNLO corrections, we do not include larger momenta in our fits.[9]

We begin with a pure NLO fit. We perform correlated fits of $\Pi^{(1)}$ to Eq. (2.4), and of $\Pi^{(1-0)}$ to Eq. (2.5), using the NLO expression for $\hat{\Pi}^{(1)}$, Eq. (2.6). Provided we include data from only the smallest valence mass, $am_v = 0.01$, we find that these fits are successful. The results are reported in Table 1. The fits in the first two rows have both L_{10} and $\Delta_{\rm mix}$ as free parameters, and favor a negative value for $\Delta_{\rm mix}$. In view of the theoretical constraint that $\Delta_{\rm mix}$ must not be negative, we repeat the fits, setting $\Delta_{\rm mix} = 0$. These fits, shown on the last two rows, retain similar statistical quality. The values of L_{10} are statistically consistent across all fits, though the fits with $\Delta_{\rm mix} = 0$ prefer a slightly larger absolute value. Averaging the results of the fits with $\Delta_{\rm mix} = 0$, the pure NLO fits give rise to

$$L_{10} = -0.0097(5) \ , \tag{3.1}$$

where the error is statistical only.

As explained above, the non-analytic NLO terms in Eq. (2.6) arise from a mixed sea-valence pion loop, which in turn depends on both the sea and valence sextet quark masses. Although the valence quark mass was held fixed (in lattice units), the NLO fits probe the fermion mass dependence thanks to the range of sea masses covered by our ensembles. Replacing the smallest valence mass by the next-smallest one, $am_v = 0.015$, gives consistent results. However, if we try to include data from the two smallest valence masses simultaneously, the fits' quality deteriorates; this stems from strong correlations in the valence spectroscopy data, as seen in the covariance matrix elements between different valence masses.

Estimating systematic uncertainties associated with a perturbative expansion is always delicate. As already mentioned in Sec. II B, going from NLO to NNLO in QCD leads to a significantly smaller value for L_{10}. We do not have data of the quality that would be needed for a full NNLO fit. Also the (complicated) non-analytic NNLO terms for our two-representation case are not available in the literature. As our best substitute for a complete NNLO analysis, we gauge its possible impact on the value of L_{10} by adding various combinations of the *analytic* NNLO terms to the basic NLO fit.

We first repeat the NLO fits, still including only the smallest valence mass, while trying out all possible combinations of the NNLO analytic terms (2.18). We find that both the mean value and the error of L_{10} vary substantially depending on the subset of the analytic NNLO terms that we include in the fit. More details of these fits may be found in App. C. This appendix also reports other exploratory studies that we have carried out.

[9] The calculation of C_{LR} in Ref. [15] involved integration of $\Pi^{(1)}(q^2)$ over all lattice momenta.

Fit	p-value	$-L_{10}$	$\Delta_{\rm mix}$	b_{vv}	b_q	b_{ss}	$-b_a$
1	0.25	0.0100(4)	–	0.196(23)	–	–	–
2	0.24	0.0098(5)	−0.04(5)	0.191(24)	–	–	–
3	0.47	0.0133(11)	–	0.189(23)	1.6(5)	–	–
4	0.44	0.0132(14)	−0.01(10)	0.187(26)	1.6(6)	–	–
5	0.31	0.0116(9)	–	0.191(23)	–	0.27(14)	–
6	0.29	0.0115(12)	−0.02(8)	0.188(25)	–	0.26(15)	–
7	0.45	0.0135(12)	–	0.188(23)	1.5(6)	0.10(15)	–
8	0.42	0.0135(16)	−0.00(12)	0.188(26)	1.5(6)	0.10(16)	–
9	0.43	0.0066(12)	–	0.190(23)	–	–	0.18(6)
10	0.41	0.0066(13)	0.01(14)	0.191(27)	–	–	0.18(7)
11	0.47	0.0106(30)	–	0.188(23)	1.1(8)	–	0.08(9)
12	0.44	0.0106(30)	0.01(15)	0.189(27)	1.1(8)	–	0.09(9)
13	0.44	0.0079(18)	–	0.188(23)	–	0.16(15)	0.16(6)
14	0.41	0.0080(18)	0.04(22)	0.192(30)	–	0.17(16)	0.16(7)
15	0.45	0.0109(30)	–	0.187(23)	1.0(8)	0.10(15)	0.08(9)
16	0.42	0.0109(30)	0.03(20)	0.190(29)	0.9(8)	0.10(17)	0.09(10)

TABLE 2. Fits of $\Pi^{(1-0)}$ to Eq. (2.5) using all 7 valence masses. The NNLO parameter b_{vv} is included in all fits. The 16 fits cover all combinations of $\Delta_{\rm mix}$ and the three remaining NNLO parameters.

In order to constrain L_{10} better, and hence to estimate the systematic error, we turn to correlated fits that include data from all seven valence masses. All fits of $\Pi^{(1)}$ to Eq. (2.4) give a p-value that is practically zero, and will not be considered any further. By contrast, fits of $\Pi^{(1-0)}$ to Eq. (2.5) turn out to give a good p-value as long as the NNLO parameter b_{vv} is present in the fit. Given the much larger valence masses included in the new fits, the need for an NNLO ingredient is not surprising. As for the difference between $\Pi^{(1)}$ and $\Pi^{(1-0)}$, we do not conclude that ChPT accounts for $\Pi^{(1-0)}$ better than $\Pi^{(1)}$. Rather, this difference stems primarily from the better behaved correlation matrix of the $\Pi^{(1-0)}$ data.

The results of the $\Pi^{(1-0)}$ fits are summarized in Table 2 and plotted in Fig. 1. All 16 fits include L_{10} and b_{vv}, and together they cover all combinations of the remaining parameters, $\Delta_{\rm mix}$, b_q, b_{ss} and b_a. With 15 ensembles and 7 valence masses, we have altogether 105 data points. The number of parameters is between 2 and 6, so that there are between 103 and 99 degrees of freedom. In spite of the fairly strong correlations still present in the $\Pi^{(1-0)}$ data, the p-value is always good.

If we look at the NNLO parameters, we see that the results for all of them are nicely consistent across all fits.[10] Indeed we find that b_{vv} is particularly stable. The NLO mixed-action parameter, $\Delta_{\rm mix}$, is always consistent with zero. The presence of $\Delta_{\rm mix}$ in the fit has virtually no effect on the mean value of L_{10}, and a very small effect on its error. We thus base our final result on the fits that do not include $\Delta_{\rm mix}$.

Turning to L_{10} itself, we see that, like the fits at the smallest valence mass (see App. C 1), different combinations of the NNLO parameters again give rise to results that vary signifi-

[10] Because of the missing NNLO non-analytic terms, we cannot quote values for NNLO LECs.

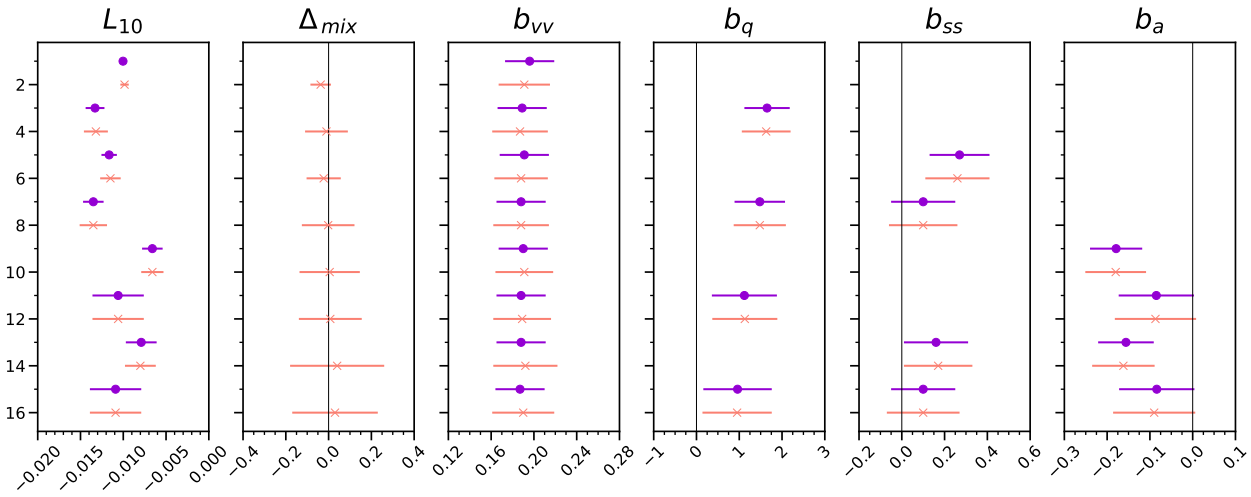

FIG. 1. Sixteen fits of $\Pi^{(1-0)}$ to data from all 7 valence masses. All fits include L_{10} and b_{vv} as parameters but have different combinations of $\Delta_{\rm mix}$ and the other NNLO parameters b_q, b_{ss} and b_a. Fits without $\Delta_{\rm mix}$ are shown in purple, and with $\Delta_{\rm mix}$ in orange. The index $i = 1, \ldots, 16$ on the ordinates corresponds to the rows of Table 1.

cantly. This means that our main source of uncertainty is systematic. In order to estimate this uncertainty, we momentarily disregard the statistical errors and consider the spread of mean values of $-L_{10}$ reported in Table 2. The highest mean value comes from fit 7, and the lowest from fit 9. The two results have similar statistical errors. We take the final mean value to be the average of fits 7 and 9, and the systematic uncertainty to be half their difference. Adding in the statistical error of the two fits, our final result is

$$L_{10} = -0.0100(12)_{\rm stat}(35)_{\rm syst} \ . \tag{3.2}$$

This result coincides with our pure NLO result (3.1), in which the error was statistical only. We note that fits 11 and 15 have a big statistical error that largely overlaps with the systematic error of our final result. These fits include all, or all but one, of the NNLO parameters, and so their statistical error probably reflects a growing redundancy among the fit parameters. As it happens, the central value stated for L_{10} coincides with the results of fits 1 and 2, where only b_{vv} is added to the NLO parameters, and the error band in Eq. (3.2) covers all the points plotted in Fig. 1. We believe that Eq. (3.2), in which the dominant error is systematic, accounts well for the behavior of L_{10} reported in Table 2.

The dominant finite-volume effects in our calculation originate in the NLO loop of the mixed valence-sea pion. Since in practice $\Delta_{\rm mix}$ vanishes, M_{vs} can be approximated by Eq. (2.7). We find that in all cases $M_{vs}L > 3.5$ and, in fact, for most of the ensembles $M_{vs}L > 4$ for all valence masses. We have performed fits similar to those reported in Table 2 but omitting the two smallest valence masses, thus achieving the stricter bound $M_{vs}L > 4$. The p-value of these fits is better than 0.75, and mostly above 0.9. In all fits, L_{10} changes by much less than 1σ. Finally, finite-volume effects in the sea sector were shown to be well under control in Ref. [11].

In QCD, it is customary to quote L_{10} at the ρ meson mass [16]. We can change the renormalization scale μ in Eq. (2.6) from $1/\sqrt{t_0}$ to the sextet vector meson mass M_{V6}. In Ref. [11] we found $M_{V6}\sqrt{t_0} \approx 0.8$ in the chiral limit [see Eq. (5.2) and Fig. 13 therein]. This would shift the central value of L_{10} by about -0.00035, a 3.5% shift.

IV. CONCLUSION

Phenomenologically, L_{10} appears in the dimension-6 lagrangian $\mathcal{L}_6$ that controls the leading deviations of Higgs decay rates from their Standard Model value [4, 6, 41]. Since only one linear combination of the parameters in $\mathcal{L}_6$ is determined by L_{10}, however, we do not pursue this calculation. On the other hand, we can use our result for L_{10} to obtain the contribution of the hypercolor sector to the S parameter, which we denote by $S_{\rm HC}$.[11] The calculation is relegated to App. A. The result is

$$S_{\rm HC} = \xi S_{\rm NLO} \ , \qquad S_{\rm NLO} = 0.8(2) \ . \tag{4.1}$$

The error of $S_{\rm NLO}$ is dominated by the systematic error of L_{10}. In contrast with technicolor models, in composite-Higgs models $S_{\rm HC}$ is suppressed [4, 6] by the vacuum misalignment parameter $\xi = 2v^2/F_6^2$, where $v = 246$ GeV is the vacuum expectation value of the Higgs field in the Standard Model, and F_6 is the decay constant of pNGBs made of the sextet fermions in the chiral limit.[12] In arriving at Eq. (4.1) we took $F_6 = 1.1$ TeV [12], the lowest value consistent with the commonly quoted upper bound $\xi \leq 0.1$ [4–6]. Also, we have assumed that all 14 pNGBs of the hypercolor theory have the same mass $M = M_h$, with $M_h = 125$ GeV the physical Higgs mass, thus obtaining an *over-estimate* of $S_{\rm NLO}$ for the given F_6.

The current experimental estimate is $S = -0.01(10)$, which implies a 1σ upper bound of 0.09 [23]. Together with Eq. (4.1) this gives an independent 1σ bound

$$\xi \leq \frac{0.09}{0.8(2)} = 0.11(3) \ . \tag{4.2}$$

Our new bound is compatible with the bound $\xi \leq 0.1$ mentioned above. It follows that the S parameter of the hypercolor theory does not lead to a more stringent constraint on the scale of new physics.

In Fig. 2 we plot $S_{\rm HC}$ as a function of the sextet decay constant F_6 in physical units, for the simplified case of degenerate pNGBs. The blue band is obtained assuming that the common pNGB mass is $M = M_h$, while for the orange band $M = 10M_h = 1.25$ TeV. We believe that, together, these bands provide an idea on $S_{\rm HC}$ for the realistic case of non-generate pNGB masses. Coming from the right, the bands cross the line $F_6 = 1.1$ TeV just before they exceed the upper bound on the S parameter, which illustrates the point that our new bound on the S parameter (4.2) is essentially the same as the existing experimental bound $\xi \leq 0.1$.

In summary, in this paper we have presented a calculation of L_{10} in a prototype composite-Higgs model, using staggered valence fermions to define the sextet-representation current correlators. We used the full NLO ChPT expressions for $\langle V_\mu V_\nu - A_\mu A_\nu \rangle$, adding analytic NNLO terms in order to estimate the systematic error. The error in our final result (3.2) is dominated by systematic uncertainties. We believe that these uncertainties can be significantly reduced only by a full-fledged NNLO calculation, a demanding task both theoretically and numerically. At a modest cost, the present calculation provides an indication of the size that L_{10} could have in similar composite-Higgs models.

For the fundamental representation, large-N_c considerations suggest that, like F_π^2, L_{10} will scale with N_c. For other representations, the expectation is that F_π^2 and L_{10} scale

[11] See, for example, Refs. [35, 36, 42].

[12] The factor of 2 in the definition of ξ stems from our normalization convention for F_6.

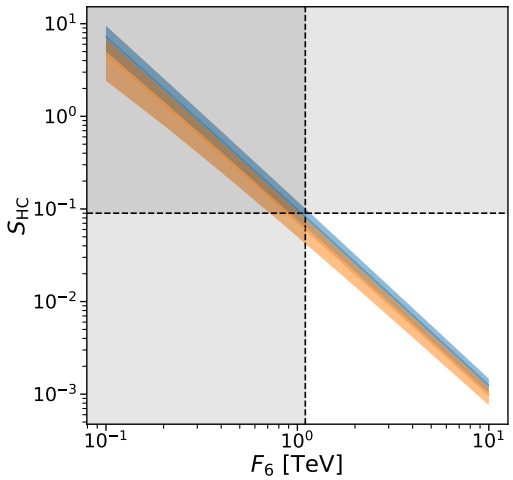

FIG. 2. Plot of $S_{\rm HC}$, the contribution of the hypercolor theory to the S parameter, as a function of the sextet decay constant F_6, assuming all pNGBs have the same mass: $M = M_h = 125$ GeV for the blue band, and $M = 10M_h$ for the orange band. $S_{\rm HC}$ depends on F_6 mainly through the vacuum misalignment parameter ξ, and hence the curves are approximately linear, with slope of -2. The horizontal line is the 1σ upper bound on the S parameter, while the vertical line gives the lower bound on F_6 compatible with the bound $\xi \leq 0.1$ (see text). Shaded areas are excluded by experiment. The curves cross into the shaded areas roughly at the point where their boundaries meet, indicating that the S parameter of the hypercolor theory does not lead to a stronger bound on ξ.

with the dimension of the representation [11]. In $N_f = 3$ QCD, the current best value is $L_{10} = -3.5(2) \times 10^{-3}$ [16, 37, 38]. Thus, our result (3.2) is reasonably consistent with the anticipated scaling.

In Ref. [14] we showed that the same prototype composite-Higgs model is unable to induce a realistic top mass via its coupling to the top partner. With two Dirac fermions in both the fundamental and sextet representations, our model is close to the M6 model of Ferretti and Karateev [7, 10]. This suggests that a realistic top mass might not be attainable in M6 either. The prospects are brighter for M11, which has more fermions in both the fundamental and sextet representations. The bigger fermion content places M11 closer to the conformal window. This, in turn, may significantly enhance the coupling between the top quark and its partner.

Acknowledgements

Our calculations of staggered fermion propagators and currents were carried out with code derived from version 7.8 of the publicly available code of the MILC collaboration [43]. Computations for this work were carried out with resources provided by the USQCD Collaboration, which is funded by the Office of Science of the U.S. Department of Energy. This material is based upon work supported by the U.S. Department of Energy, Office of Science, Office of High Energy Physics, under Awards No. DE-SC0010005 (Colorado) and DE-SC0013682 (SFSU), and by the Israel Science Foundation under grant No. 491/17 (Tel Aviv). Fermilab is operated by the Fermi Research Alliance, LLC under contract No. DE-AC02-07CH11359 with the U.S. Department of Energy.

Appendix A: S parameter

For a real representation, the non-linear field is symmetric, $\Sigma = \Sigma^T$, and takes values in $\mathrm{SU}(N_M)$, where N_M is the number of Majorana fermions. The symmetry breaking pattern is $\mathrm{SU}(N_M) \to \mathrm{SO}(N_M)$ [44], and, assuming that the vacuum $\langle\Sigma\rangle$ is aligned with the identity matrix, the generators of $\mathrm{SO}(N_M)$ are antisymmetric.

L_{10} couples to the NLO operator [20]

$$\mathcal{O}_{10}^{\mathrm{real}} = \mathrm{tr}\left(\mathcal{B}_{\mu\nu}\Sigma\mathcal{B}_{\mu\nu}^T\Sigma^*\right) \ , \tag{A1}$$

where the external gauge field $\mathcal{B}_{\mu\nu}$ promotes the full $\mathrm{SU}(N_M)$ flavor symmetry group to a local symmetry. For the calculation of L_{10}, as well as the S parameter, we only need the linearized part of $\mathcal{B}_{\mu\nu}$. Writing $\mathcal{B}_{\mu\nu} = \mathcal{V}_{\mu\nu} - \mathcal{A}_{\mu\nu}$, with $\mathcal{V}_{\mu\nu}$ ($\mathcal{A}_{\mu\nu}$) for the unbroken (broken) generators, we arrive at Eq. (1.1), which has the same form as in the familiar QCD case.[13] In terms of $\langle V_\mu V_\nu - A_\mu A_\nu\rangle$, the S parameter may be defined for any fermion representation as [20, 22]

$$S = -2\pi \lim_{q^2\to 0} \frac{\partial}{\partial q^2}\, q^2\Pi^{(1)} = -2\pi \lim_{q^2\to 0} \hat{\Pi}^{(1)} \ . \tag{A2}$$

At NLO this gives

$$S_{\mathrm{NLO}} = -\frac{\mathcal{G}(N)}{24\pi}\left(1 + \log\left(\frac{M^2}{\mu^2}\right)\right) - 16\pi L_{10} \ , \tag{A3}$$

where we have used Eq. (2.6), and $\lim_{q^2\to 0} H(s) = -2/3$. Starting from the renormalization scale $\mu = 1/\sqrt{t_0}$ used in Sec. III, it will be convenient to reexpress $\log(t_0 M^2) = \log(M^2/F_6^2) + \log(t_0 F_6^2)$, where F_6 is the decay constant of the sextet fermions in the chiral limit, using $\sqrt{t_0}F_6 = 0.17(1)$ [11].

In order to assess the phenomenological impact of our calculation we consider the actual M6 model [8]. As mentioned in the introduction, this model has 5 Majorana fermions in the sextet representation of the SU(4) gauge theory. The global symmetry of the sextet sector is SU(5), and the unbroken symmetry is SO(5) before the coupling to the Standard Model fields is turned on. We will assume that the actual value of L_{10} in the sextet sector of this hypercolor theory is close to what we find in our lattice model, Eq. (3.2). When applying Eq. (A3) to the M6 model, we will use $\mathcal{G}(N) = \mathcal{G}(5/2) = 7/2$.

The $\mathrm{SU}(2)_L \times \mathrm{SU}(2)_R$ symmetry of the Standard Model is identified with an SO(4) subgroup of the unbroken SO(5), with the $\mathrm{SU}(2)_L$ gauge fields W_μ^i, $i = 1, 2, 3$, coupled to the generators T_L^i, and the $\mathrm{U}(1)_Y$ gauge field B_μ coupled to T_R^3. The Higgs doublet is identified with 4 pNGBs of the coset SU(5)/SO(5). After electroweak symmetry breaking, the vacuum of the sextet sector becomes $\langle\Sigma\rangle = \Omega^2(\zeta)$, where the argument of Ω is $\zeta = \sqrt{2}h/F_6$, with h the expectation value of the pNGB field associated with the physical Higgs particle. The explicit form of Ω, as well as of the $\mathrm{SU}(2)_{L,R}$ generators $T_{L,R}^i$, may be found in Appendix B of Ref. [8].

Experimentally, the S parameter is defined as the contribution of new physics beyond the Standard Model to Eq. (A2), where, instead of $\langle V_\mu V_\nu - A_\mu A_\nu\rangle$, the transverse function $\Pi^{(1)}$ is defined from the correlator $\left\langle J_\mu^{W_3} J_\nu^B \right\rangle$ [4, 6, 22, 23]. The contribution of the hypercolor theory to the S parameter, denoted S_{HC}, is given at NLO by [compare Eq. (4.1)]

$$S_{\mathrm{HC}} = \xi S_{\mathrm{NLO}} \ , \tag{A4}$$

[13] For more details, see Refs. [20, 21, 45] and references therein.

where $S_{\rm NLO}$ is calculated in the hypercolor theory using Eq. (A3); the vacuum misalignment parameter is

$$\xi \equiv \frac{2v^2}{F_6^2} = \sin^2(\sqrt{2}h/F_6) \ . \tag{A5}$$

In arriving at Eq. (A4) we used

$$\mathrm{tr}\left(T_L^i \Omega^2 T_R^j (\Omega^2)^*\right) = \xi \delta_{ij} \ . \tag{A6}$$

In Eq. (A3) we have made the simplifying assumption that the 14 pNGBs of the coset SU(5)/SO(5) are all degenerate in mass. In reality, apart from any explicit mass terms in the hypercolor theory, the coupling to Standard Model fields will generate an effective potential [4–6, 8–10, 24, 25], whose minimization must generate an expectation value for the Higgs field. Then the pNGBs split into several distinct multiplets of the $\mathrm{SU}(2)_V$ diagonal subgroup of $\mathrm{SU}(2)_L \times \mathrm{SU}(2)_R$. The Higgs doublet contains the physical Higgs field and the 3 NGBs of $\mathrm{SU}(2)_L \times \mathrm{SU}(2)_R \to \mathrm{SU}(2)_V$ symmetry breaking. The other 10 pNGBs split into two singlets, a triplet, and a quintet of $\mathrm{SU}(2)_V$. Furthermore, the coupling to the $\mathrm{U}(1)_Y$ gauge field breaks explicitly $\mathrm{SU}(2)_R$, and thus also $\mathrm{SU}(2)_V$, generating additional mass splittings depending on the electric charges,[14] which in turn range from 0 to ± 2. The electrically charged pNGBs must have large masses to evade detection. Thus, calculating $S_{\rm NLO}$ for the realistic non-degenerate case is tedious, and the resulting expression will depend on several unknown masses. Instead, we calculate $S_{\rm NLO}$ in the conclusion section for the degenerate mass case using Eq. (A3). To get an idea of the variation of the S parameter as a function of the pNGB masses, we calculate it for two distinct choices of the common pNGB mass M.

Appendix B: NNLO discretization effects

In this appendix we explain why the NNLO discretization term in Eq. (2.18) is $O(a^2)$, and not $O(a)$. In itself, an a^2 discretization term is consistent with the usual power counting of staggered ChPT. Since, however, our mixed-action calculation also includes Wilson (sea) fermions, the question arises whether there should be an $O(a)$ discretization term in Eq. (2.18).

Wilson ChPT comes with two alternative power counting schemes for the discretization effects, known as GSM, where $m \sim a$, and LCE, where $m \sim a^2$ (see for example Ref. [33]). Here we follow the GSM scheme, as we did in our spectroscopy study [11]. The LO potential for pions made out of Wilson fermions is then [46]

$$\mathcal{L}_m = -\frac{F^2 B m'}{2} \mathrm{tr}(\Sigma + \Sigma^\dagger) \ . \tag{B1}$$

The shifted mass m' is defined by

$$Bm' = Bm + W_0 a \ , \tag{B2}$$

where B is the usual continuum LEC, while W_0 is a new LEC peculiar to Wilson ChPT.

A central feature is the relation between the shifted mass m' and the axial Ward identity mass $m_{\rm AWI}$. The latter is defined by *imposing* the following identity in the Wilson theory,

$$\partial_4 \langle A_4^a(t) P^a(0) \rangle = 2 m_{\rm AWI} \langle P^a(t) P^a(0) \rangle \ , \tag{B3}$$

[14] The 3 exact NGBs turn into the longitudinal components of the $W^\pm$ and Z bosons.

where the correlation functions are evaluated at zero spatial momentum. A_μ^a and P^a are the renormalized (and, possibly, improved) axial current and pseudoscalar density of the Wilson theory. In Ref. [47] the following relation was proved between the shifted mass m' and $m_{\rm AWI}$,

$$m_{\rm AWI} = m' + O(m^2) + O(ma) + O(a^2) \ . \tag{B4}$$

Notice the absence of an $O(a)$ term on the right-hand side; the $O(a)$ term from Eq. (B2) has been absorbed into m'. Physically, Eq. (B3) implies that the mass of the Wilson pion satisfies $M_\pi^2 \sim m_{\rm AWI}$, whereas Wilson ChPT at LO implies the relation $M_\pi^2 \sim m'$. Thus, Eq. (B4) expresses the consistency of Wilson ChPT with the underlying theory.

If we tune the shifted mass to zero, it follows that $m = O(a)$, and so

$$m_{\rm AWI} = O(a^2) \ , \qquad m' \to 0 \ . \tag{B5}$$

In words, $m_{\rm AWI}$ vanishes simultaneously with the shifted mass, up to a residual $O(a^2)$ part. The leftover $O(a^2)$ term is important, as it leaves room for the Aoki phase [46, 48]. In particular, within the so-called 1st-order scenario [46], $m_{\rm AWI}$ and M_π^2 do not vanish at $m' = 0$. Rather, they attain $O(a^2)$ minimum values there, and their m' derivatives are discontinuous.

In our mixed-action case, only two terms in the chiral lagrangian are relevant to this discussion, namely,

$$(\tilde{B}m + \tilde{W}a)\,\mathrm{tr}\Big(P_s(\Sigma + \Sigma^\dagger)\Big)\,\mathrm{tr}\Big((\mathcal{V}_{\mu\nu} - \mathcal{A}_{\mu\nu})P_v\Sigma(\mathcal{V}_{\mu\nu} + \mathcal{A}_{\mu\nu})P_v\Sigma^\dagger\Big) \ , \tag{B6}$$

where $\tilde{B}$ and $\tilde{W}$ are new NNLO LECs. The chiral field Σ now accounts for the sea, valence, and ghost quarks. The corresponding projectors—P_s, P_v and P_{gh}, respectively—satisfy $P_s + P_v + P_{gh} = 1$. With these projectors in place, the first trace has the same form as the Wilson LO potential (B1), whereas the second trace reduces to the L_{10} operator (1.1) acting on the valence entries of the Σ field.

The key observation is that [by Eq. (B5)] when we tune $m' \to 0$ the remaining chiral symmetry violations of the Wilson theory are $O(a^2)$. In order that no $O(a)$ violations will survive in this limit, we must have

$$\tilde{B}m + \tilde{W}a = \tilde{B}m' \tag{B7}$$

in Eq. (B6). To see this, we may consider the Ward–Takahashi identity

$$\partial_4 \left\langle A_{4,s}^a(t) P_s^a(0) J_{v,\mu b}^L J_{v,\mu b}^R \right\rangle = 2m_{\rm AWI} \left\langle P_s^a(t) P_s^a(0) J_{v,\mu b}^L J_{v,\mu b}^R \right\rangle \ , \tag{B8}$$

where the subscripts s, v refer to sea and valence operators, respectively [cf. Eq. (2.14)]. In the mixed-action theory, this Ward–Takahashi identity corresponds to an axial transformation in the Wilson sea sector only. Since the valence operators in Eq. (B8) are inert under this transformation, consistency with Eq. (B3) requires that the coefficient on the right-hand side must be $2m_{\rm AWI}$. Furthermore, in order that the identity be reproduced in mixed-action ChPT, Eq. (B7) must be true. The prefactor in Eq. (B6) is therefore proportional to the shifted mass, and a separate $O(a)$ term cannot be present.

Appendix C: Other methods

In this appendix we briefly describe several alternative fits that we have carried out for the determination of L_{10}. With the notable exception of the pure NLO fits already discussed in Sec. III, the results are inferior in quality to the preferred analyses presented in the body of the paper.

1. Fits with the lightest valence mass

Our NLO fits using the lightest valence mass were discussed in Sec. III. As briefly mentioned there, we also considered the effect of adding NNLO analytic terms to the basic NLO fit. We performed correlated fits of $\Pi^{(1)}$ to Eq. (2.4); alternatively, we fit $\Pi^{(1-0)}$ to Eq. (2.5). The left panel of Fig. 3 shows the values of L_{10} obtained from fits of $\Pi^{(1)}$ with all combinations of the NNLO parameters [Eq. (2.18)], both with and without the parameter $\Delta_{\rm mix}$ [Eq. (2.17)]. The four columns of $+/-$ signs indicate which NNLO parameters are present/absent in each fit. In each case we plot a fit that includes $\Delta_{\rm mix}$ in blue, and a fit where we set $\Delta_{\rm mix} = 0$ in red. The results of fitting $\Pi^{(1-0)}$ are presented similarly in the right panel of Fig. 3, using the same color scheme. All fits are of good quality, with p-values in the range 0.25–0.8.

A comparison of the two panels of Fig. 3 shows that there is generally good agreement between the values of L_{10} obtained from each fit to $\Pi^{(1)}$, and from the corresponding fit to $\Pi^{(1-0)}$. The pure NLO fits (the topmost fit in each panel) have small statistical errors—roughly the size of the symbol. When we add NNLO analytic terms, both the mean value and the error of L_{10} vary substantially depending on which additional parameters are present in the fit. As we explained in Sec. II B and Sec. III, when it comes to estimating the systematic effect of the missing non-analytic NNLO terms, *a priori* any combination of NNLO parameters is as good as any other. With their error bars, the results displayed in Fig. 3 would allow L_{10} to be basically anywhere in the range $[-0.035, 0.0]$. By contrast, the fits with all 7 valence masses presented in Sec. III constrain L_{10} with a much smaller systematic error, at the modest price of always having to include the NNLO parameter b_{vv} in the fit.

2. Using ChPT for F_{vv}

The pole parts in Eqs. (2.4) and (2.5) are proportional to the valence decay constant squared, F_{vv}^2. Instead of taking F_{vv} from data, we may alternatively use the NLO expression,

$$\sqrt{t_0} F_{vv,6} = \mathring{F}_6 \left[(1 - 2\Delta_6) + t_0 \left(L_{66}^{vs} M_{ss,6}^2 + L_{64}^{vs} M_{ss,4}^2 + L_{66}^{vv} M_{vv,6}^2 \right) \right] + L_6^{\rm latt} \hat{a}^2 \ . \tag{C1}$$

The notation here is similar to Ref. [11] (see also Ref. [21]). The subscripts 4 and 6 refer to the fundamental and sextet representations, respectively. $\mathring{F}_6$ is the sextet decay constant in the chiral limit in t_0 units, while L_{66}^{vs}, L_{64}^{vs}, L_{66}^{vv} and $L_6^{\rm latt}$ are linear combinations of various NLO LECs. The NLO logarithm is

$$\Delta_6 = \frac{t_0 M_{vs,6}^2}{8\pi^2 \mathring{F}_6^2} \log(t_0 M_{vs,6}^2) \ . \tag{C2}$$

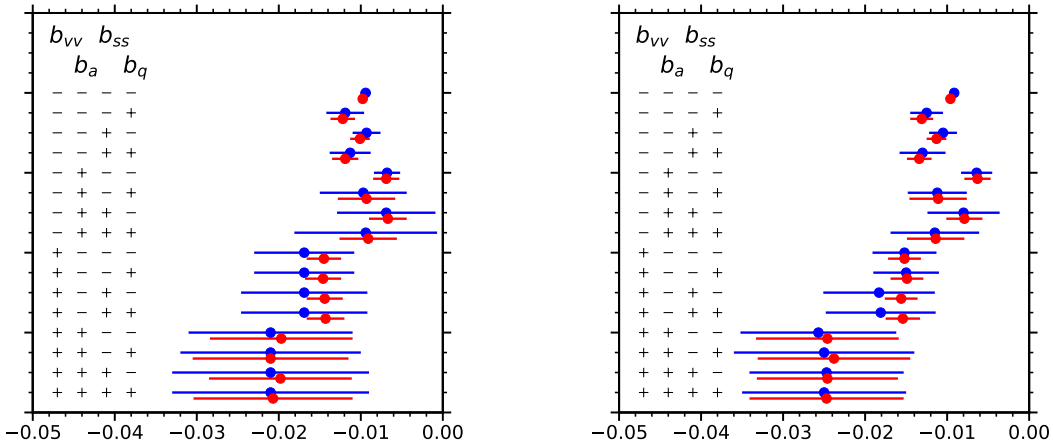

FIG. 3. Results for L_{10}, using only the smallest valence mass $am_v = 0.01$, for all combinations of the four NNLO parameters and $\Delta_{\rm mix}$ (see App. C 1). Left panel: Fits of $\Pi^{(1)}$. Right panel: fits of $\Pi^{(1-0)}$. The columns with $+/-$ signs indicate which NNLO parameters are present/absent in each fit. Fit results with $\Delta_{\rm mix}$ free are shown in blue, and fits with $\Delta_{\rm mix} = 0$ in red. The topmost pair of points in each plot represents the NLO fit.

This logarithm is the same as in Ref. [11], except that the pion in the loop is now a mixed sea-valence pion. Note the absence of a discretization term $\sim a$, which can be proved using arguments similar to those in App. B.

Fits using the above expression for $F_{vv} = F_{vv,6}$ are largely consistent with our final result for L_{10}, Eq. (3.2). However, the uncertainty in the value of L_{10} turns out to be much larger here, and therefore we do not include fits that make use of Eq. (C1) in our main analysis.

The sextet decay constant in the chiral limit, $\mathring{F}_6$, which is one of the fit parameters in Eq. (C1), was already determined in Ref. [11]. The result we find here for $\mathring{F}_6$ is consistent with the value reported in Ref. [11], albeit with a larger error.

One could similarly carry out fits using the NLO expressions for both F_{vv} and M_{vv} in the pole term of $\Pi^{(1-0)}$. In view of the limited success of the fits using Eq. (C 2) we do not pursue such fits. We comment that in the case of M_{vv} one expects larger finite-volume effects, originating from "hairpin" diagrams with a valence pion in the loop. In the fits reported in Sec. III we take both F_{vv} and M_{vv} from data, and hence this issue does not arise.

3. Prior extrapolation to the $m_v \to 0$ limit

We showed in App. C 1 the result of fitting only the smallest valence mass for each ensemble. This was motivated by a desire to distill highly correlated data down to a single data point for each ensemble. An alternative, similarly motivated, is to extrapolate $\Pi^{(1)}$ to the chiral-valence limit, leaving us with $\Pi^{(1)}(am_v \to 0)$ for each ensemble. We have performed the extrapolations via uncorrelated linear fits. The linearity of the extrapolation, and the use of independent fit parameters for each ensemble, both mean that this is not ChPT. Still, the linear extrapolations turn out to have some interesting features all by themselves.

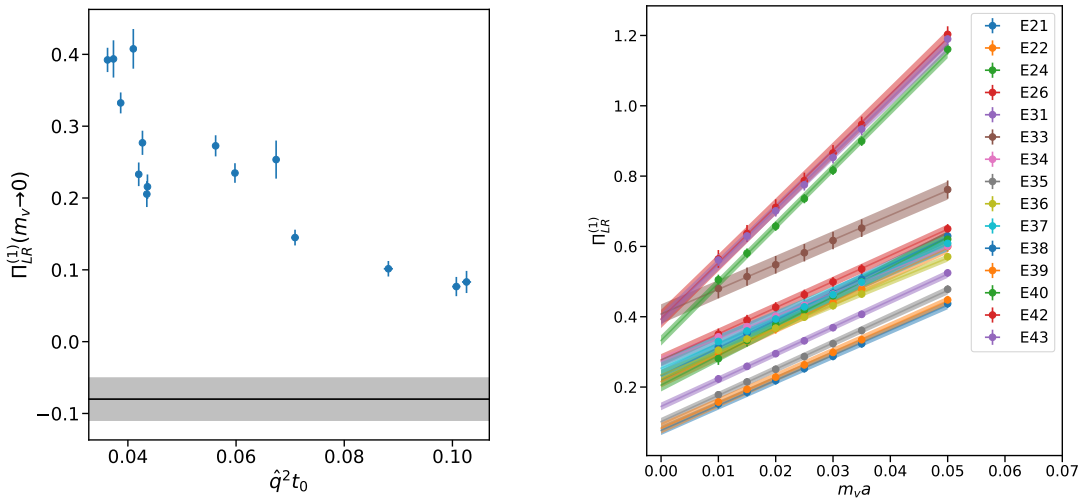

FIG. 4. Left: $\Pi^{(1)}$ in the chiral-valence limit $am_v \to 0$ plotted against $\hat{q}^2 t_0$ for all 15 ensembles. The horizontal grey band shows the contribution $8L_{10}$ to $\Pi^{(1)}(q)$, where for simplicity we combined the statistical and systematic errors of our final result in quadrature [see Eq. (3.2)]. Right: The linear fits of $\Pi^{(1)}$ in each ensemble that give the limits shown on the left. Ensemble numbers are as in Ref. [11].

The results are shown in the left panel of Fig. 4, plotted against $\hat{q}^2 t_0$ for each of the 15 ensembles. Note that while the dimensionless $q_\mu a$ is always the smallest time-like momentum, the gradient-flow scale t_0/a^2 varies considerably between ensembles. The jaggedness of the plot is because $\Pi^{(1)}(am_v \to 0)$ depends not only on $\hat{q}^2 t_0$, but also on the sea sextet fermion mass, as well as (weakly) on the sea fundamental fermion mass. To give a visual impression, the contribution $8L_{10}$ to $\Pi^{(1)}(q)$ is shown as a horizontal grey band, using the final result (3.2), with statistical and systematic error added in quadrature [see Eqs. (2.4) and (2.6)].

The actual linear extrapolations are shown in the right panel of Fig. 4. The first thing to notice is that, visually, the linear fits describe the data well. A distinct feature of these linear fits is that almost the same slope is found for all the $16^3 \times 32$ ensembles; the three larger $24^3 \times 28$ ensembles (E40, E42 and E43) again exhibit a similar slope, which in turn is bigger than that of the $16^3 \times 32$ ensembles.

The dependence of the slopes on the lattice size appears to arise primarily from the kinematical pole, $F_{vv}^2/\hat{q}^2$ (recall we are using only the smallest timelike momentum). We have checked that $(aF_{vv})^2$ is also roughly linear in am_v, with again, almost the same slope for all the $16^3 \times 32$ ensembles, and with a different slope for all the $24^3 \times 28$ ensembles. The slope for the $16^3 \times 32$ ensembles is in fact larger than the slope for the $24^3 \times 28$ ensembles; but this trend is reversed once $(aF_{vv})^2$ is divided by $a^2\hat{q}^2$, a geometrical factor which is smaller for the ensembles with the larger volume.

In Sec. III we carried out successful correlated fits of $\Pi^{(1-0)}$ to the ChPT expressions of Sec. II, using data from all seven valence masses. The importance of the m_v dependence is evident from the fact that we had to include a term $\propto M_{vv}^2$ in all those fits, if we remember that M_{vv}^2 and m_v are interchangeable at this order. Using for definiteness the parameters of fit 1 from Table 2, we confirm that there is visually good agreement between data and

fit for $\Pi^{(1)}$. This means that ChPT is capable of reproducing the roughly linear behavior of $\Pi^{(1)}$ exhibited in the right panel of Fig. 4.

In summary, the fits based on the $m_v \to 0$ extrapolations reveal some interesting features of the data, which are explained *a posteriori* by ChPT. Because *a priori* these fits represent a departure from ChPT, we did not include them in our main analysis.

---

[1] H. Georgi and D. B. Kaplan, *Composite Higgs and Custodial SU(2),* Phys. Lett. B **145**, 216 (1984).

[2] M. J. Dugan, H. Georgi and D. B. Kaplan, *Anatomy of a Composite Higgs Model,* Nucl. Phys. B **254**, 299 (1985).

[3] D. B. Kaplan, *Flavor at SSC energies: A New mechanism for dynamically generated fermion masses,* Nucl. Phys. B **365**, 259 (1991).

[4] R. Contino, *The Higgs as a Composite Nambu-Goldstone Boson,* in *Physics of the Large and the Small, TASI 09, Proceedings of the Theoretical Advanced Study Institute in Elementary Particle Physics, Boulder, Colorado, USA, 2009 (World Scientific, Singapore, 2011)*, pp. 235–306 [arXiv:1005.4269 [hep-ph]].

[5] B. Bellazzini, C. Csáki and J. Serra, *Composite Higgses,* Eur. Phys. J. C **74**, no. 5, 2766 (2014) [arXiv:1401.2457 [hep-ph]].

[6] G. Panico and A. Wulzer, *The Composite Nambu-Goldstone Higgs,* Lect. Notes Phys. **913**, pp.1 (2016) [arXiv:1506.01961 [hep-ph]].

[7] G. Ferretti and D. Karateev, *Fermionic UV completions of Composite Higgs models,* JHEP **1403**, 077 (2014) [arXiv:1312.5330 [hep-ph]].

[8] G. Ferretti, *UV Completions of Partial Compositeness: The Case for a SU(4) Gauge Group,* JHEP **1406**, 142 (2014) [arXiv:1404.7137 [hep-ph]].

[9] G. Ferretti, *Gauge theories of Partial Compositeness: Scenarios for Run-II of the LHC,* JHEP **1606**, 107 (2016) [arXiv:1604.06467 [hep-ph]].

[10] A. Belyaev, G. Cacciapaglia, H. Cai, G. Ferretti, T. Flacke, A. Parolini and H. Serodio, *Di-boson signatures as Standard Candles for Partial Compositeness,* JHEP **1701**, 094 (2017) [arXiv:1610.06591 [hep-ph]].

[11] V. Ayyar, T. DeGrand, M. Golterman, D. C. Hackett, W. I. Jay, E. T. Neil, Y. Shamir and B. Svetitsky, *Spectroscopy of SU(4) composite Higgs theory with two distinct fermion representations,* Phys. Rev. D **97**, no. 7, 074505 (2018) [arXiv:1710.00806 [hep-lat]].

[12] V. Ayyar, T. Degrand, D. C. Hackett, W. I. Jay, E. T. Neil, Y. Shamir and B. Svetitsky, *Baryon spectrum of SU(4) composite Higgs theory with two distinct fermion representations,* Phys. Rev. D **97**, no. 11, 114505 (2018) [arXiv:1801.05809 [hep-ph]].

[13] V. Ayyar, T. DeGrand, D. C. Hackett, W. I. Jay, E. T. Neil, Y. Shamir and B. Svetitsky, *Finite-temperature phase structure of SU(4) gauge theory with multiple fermion representations,* Phys. Rev. D **97**, no. 11, 114502 (2018) [arXiv:1802.09644 [hep-lat]].

[14] V. Ayyar, T. DeGrand, D. C. Hackett, W. I. Jay, E. T. Neil, Y. Shamir and B. Svetitsky, *Partial compositeness and baryon matrix elements on the lattice,* Phys. Rev. D **99**, no. 9, 094502 (2019) [arXiv:1812.02727 [hep-ph]].

[15] V. Ayyar, M. Golterman, D. C. Hackett, W. Jay, E. T. Neil, Y. Shamir and B. Svetitsky, *Radiative Contribution to the Composite-Higgs Potential in a Two-Representation Lattice Model,* Phys. Rev. D **99**, no.9, 094504 (2019) [arXiv:1903.02535 [hep-lat]].

[16] S. Aoki *et al.* [Flavour Lattice Averaging Group], *FLAG Review 2019: Flavour Lattice Averaging Group (FLAG),* Eur. Phys. J. C **80**, no.2, 113 (2020) [arXiv:1902.08191 [hep-lat]].

[17] T. DeGrand and C. DeTar, *Lattice Methods for Quantum Chromodynamics,* (World Scientific, Singapore, 2006).

[18] E. Bennett, D. K. Hong, J. W. Lee, C. J. D. Lin, B. Lucini, M. Piai and D. Vadacchino, *Sp(4) gauge theory on the lattice: towards SU(4)/Sp(4) composite Higgs (and beyond),* JHEP **03**, 185 (2018) [arXiv:1712.04220 [hep-lat]]; *Sp(4) gauge theories on the lattice: $N_f = 2$ dynamical fundamental fermions,* JHEP **12**, 053 (2019) [arXiv:1909.12662 [hep-lat]]. E. Bennett, D. K. Hong, J. W. Lee, C. J. D. Lin, B. Lucini, M. Mesiti, M. Piai, J. Rantaharju and D. Vadacchino, *Sp*(4) *gauge theories on the lattice: quenched fundamental and antisymmetric fermions,* Phys. Rev. D **101**, no.7, 074516 (2020) [arXiv:1912.06505 [hep-lat]].

[19] J. Gasser and H. Leutwyler, *Chiral Perturbation Theory: Expansions in the Mass of the Strange Quark,* Nucl. Phys. B **250**, 465 (1985).

[20] J. Bijnens and J. Lu, *Two-Point Functions and S-Parameter in QCD-like Theories,* JHEP **1201**, 081 (2012) [arXiv:1111.1886 [hep-ph]].

[21] T. DeGrand, M. Golterman, E. T. Neil and Y. Shamir, *One-loop Chiral Perturbation Theory with two fermion representations,* Phys. Rev. D **94**, no. 2, 025020 (2016) [arXiv:1605.07738 [hep-ph]].

[22] M. E. Peskin and T. Takeuchi, *Estimation of oblique electroweak corrections,* Phys. Rev. D **46**, 381-409 (1992)

[23] P. A. Zyla *et al.* [Particle Data Group], *Review of Particle Physics,* PTEP **2020**, no.8, 083C01 (2020)

[24] M. Golterman and Y. Shamir, *Top quark induced effective potential in a composite Higgs model,* Phys. Rev. D **91**, no. 9, 094506 (2015) [arXiv:1502.00390 [hep-ph]].

[25] M. Golterman and Y. Shamir, *Effective potential in ultraviolet completions for composite Higgs models,* Phys. Rev. D **97**, no. 9, 095005 (2018) [arXiv:1707.06033 [hep-ph]].

[26] E. Golowich and J. Kambor, *Two loop analysis of vector current propagators in chiral perturbation theory,* Nucl. Phys. B **447**, 373 (1995) [hep-ph/9501318].

[27] G. Amoros, J. Bijnens and P. Talavera, *Two point functions at two loops in three flavor chiral perturbation theory,* Nucl. Phys. B **568**, 319 (2000) [hep-ph/9907264].

[28] O. Bär, G. Rupak and N. Shoresh, *Chiral perturbation theory at O(a**2) for lattice QCD,* Phys. Rev. D **70**, 034508 (2004) [arXiv:hep-lat/0306021 [hep-lat]].

[29] O. Bär, C. Bernard, G. Rupak and N. Shoresh, *Chiral perturbation theory for staggered sea quarks and Ginsparg-Wilson valence quarks,* Phys. Rev. D **72**, 054502 (2005) [arXiv:hep-lat/0503009 [hep-lat]].

[30] J. W. Chen, M. Golterman, D. O'Connell and A. Walker-Loud, *Mixed Action Effective Field Theory: An Addendum,* Phys. Rev. D **79**, 117502 (2009) [arXiv:0905.2566 [hep-lat]].

[31] O. Bär, M. Golterman and Y. Shamir, *Flavor symmetry breaking in lattice QCD with a mixed action,* Phys. Rev. D **83**, 054501 (2011) [arXiv:1012.0987 [hep-lat]].

[32] G. Ecker, *The Standard model at low-energies,* Czech. J. Phys. **44**, 405 (1994) [hep-ph/9309268].

[33] M. Golterman, *Applications of chiral perturbation theory to lattice QCD,* in *Modern perspectives in lattice QCD: Quantum field theory and high performance computing*, Proceedings, International School, 93rd Session, Les Houches, France, August 3-28, 2009 (Oxford University Press, 2011) pp. 423–515 [arXiv:0912.4042 [hep-lat]].

[34] M. Lüscher, *Properties and uses of the Wilson flow in lattice QCD,* JHEP **08**, 071 (2010)

[arXiv:1006.4518 [hep-lat]].

[35] E. Shintani *et al.* [JLQCD Collaboration], *S-parameter and pseudo-Nambu-Goldstone boson mass from lattice QCD,* Phys. Rev. Lett. **101**, 242001 (2008) [arXiv:0806.4222 [hep-lat]].

[36] P. A. Boyle *et al.* [RBC and UKQCD Collaborations], *The S Parameter in QCD from Domain Wall Fermions,* Phys. Rev. D **81**, 014504 (2010) [arXiv:0909.4931 [hep-lat]].

[37] D. Boito, A. Francis, M. Golterman, R. Hudspith, R. Lewis, K. Maltman and S. Peris, *Low-energy constants and condensates from ALEPH hadronic τ decay data,* Phys. Rev. D **92**, no. 11, 114501 (2015) [arXiv:1503.03450 [hep-ph]].

[38] P. A. Boyle, L. Del Debbio, N. Garron, R. J. Hudspith, E. Kerrane, K. Maltman and J. M. Zanotti, *Combined NNLO lattice-continuum determination of L^r_{10},* Phys. Rev. D **89** (2014) no.9, 094510 [arXiv:1403.6729 [hep-ph]].

[39] A. Bazavov *et al.* [MILC Collaboration], *Nonperturbative QCD Simulations with 2+1 Flavors of Improved Staggered Quarks,* Rev. Mod. Phys. **82**, 1349 (2010) [arXiv:0903.3598 [hep-lat]].

[40] T. A. DeGrand, M. Golterman, W. I. Jay, E. T. Neil, Y. Shamir and B. Svetitsky, *Radiative contribution to the effective potential in composite Higgs models from lattice gauge theory,* Phys. Rev. D **94**, no.5, 054501 (2016) [arXiv:1606.02695 [hep-lat]].

[41] G. F. Giudice, C. Grojean, A. Pomarol and R. Rattazzi, *The Strongly-Interacting Light Higgs,* JHEP **0706**, 045 (2007) [hep-ph/0703164].

[42] T. Appelquist *et al.* [LSD], *Parity Doubling and the S Parameter Below the Conformal Window,* Phys. Rev. Lett. **106**, 231601 (2011) [arXiv:1009.5967 [hep-ph]].

[43] MILC Collaboration, `http://www.physics.utah.edu/~detar/milc/`

[44] M. E. Peskin, *The Alignment of the Vacuum in Theories of Technicolor,* Nucl. Phys. B **175**, 197-233 (1980)

[45] M. Golterman and Y. Shamir, *Phase ambiguity of the measure for continuum Majorana fermions,* Phys. Rev. D **100**, no.3, 034507 (2019) [arXiv:1904.08600 [hep-lat]].

[46] S. R. Sharpe and R. L. Singleton, Jr, *Spontaneous flavor and parity breaking with Wilson fermions,* Phys. Rev. D **58**, 074501 (1998) [arXiv:hep-lat/9804028 [hep-lat]].

[47] S. Aoki, O. Bär and S. R. Sharpe, *Vector and Axial Currents in Wilson Chiral Perturbation Theory,* Phys. Rev. D **80**, 014506 (2009) [arXiv:0905.0804 [hep-lat]].

[48] S. Aoki, *New Phase Structure for Lattice QCD with Wilson Fermions,* Phys. Rev. D **30**, 2653 (1984); *A Solution to the U(1) Problem on a Lattice,* Phys. Rev. Lett. **57**, 3136 (1986); *On the phase structure of QCD with Wilson fermions,* Prog. Theor. Phys. Suppl. **122**, 179-186 (1996) [arXiv:hep-lat/9509008 [hep-lat]].